

Modeling the 2010 blast wave of the symbiotic-like nova V407 Cygni

Salvatore Orlando¹ *, Jeremy J. Drake²

¹INAF - Osservatorio Astronomico di Palermo “G.S. Vaiana”, Piazza del Parlamento 1, 90134, Palermo, Italy

²Harvard-Smithsonian Center for Astrophysics, 60 Garden Street, Cambridge, MA 02138, USA

Accepted. Received

ABSTRACT

The symbiotic-like binary Mira and nova V407 Cyg was observed in outburst on March 2010 and monitored in several wavelength bands. The outburst had, to some extent, characteristics similar to those observed during other nova eruptions, such as recently occurred in RS Oph and U Sco, suggesting that the blast wave interacted with the giant companion and propagated through a dense circumstellar medium enveloping the binary system. Here we report on multi-dimensional hydrodynamic simulations describing the 2010 outburst of V407 Cyg, exploring the first 60 days of evolution. The model takes into account thermal conduction (including the effects of heat flux saturation) and radiative cooling; the pre-explosion system conditions included the companion star and a circumbinary density enhancement that are believed to influence the evolution and morphology of the blast wave. The simulations showed that the blast and the ejecta distribution are both aspherical due to the inhomogeneous circumstellar medium in which they expand; in particular they are significantly collimated in polar directions (producing a bipolar shock morphology) if the circumstellar envelope is characterized by an equatorial density enhancement. The blast is partially shielded by the Mira companion, producing a wake with dense and hot post-shock plasma on the rear side of the companion star; most of the X-ray emission produced during the evolution of the blast arises from this plasma structure. The observed X-ray lightcurve can be reproduced, assuming values of outburst energy and ejected mass similar to those of RS Oph and U Sco, if a circumbinary gas density enhancement is included in the model. In particular, our “best-fit” model predicts that the 2010 blast propagated through a circumbinary gas density enhancement with radius of the order of 40 AU and gas density $\approx 10^6 \text{ cm}^{-3}$ and that the mass of ejecta in the outburst was $M_{\text{ej}} \approx 2 \times 10^{-7} M_{\odot}$ with an explosion energy $E_0 \approx 2 \times 10^{44} \text{ erg}$. Alternatively, the model can produce a similar X-ray lightcurve without the need of a circumbinary gas density enhancement only if the outburst energy and ejected mass were similar to those at the upper end of ranges for classical novae, namely $M_{\text{ej}} \approx 5 \times 10^{-5} M_{\odot}$ and $E_0 \approx 5 \times 10^{46} \text{ erg}$.

Key words: shock waves – binaries: symbiotic – circumstellar matter – stars: individual (V407 Cyg) – novae, cataclysmic variables – X-rays: binaries

1 INTRODUCTION

The symbiotic binary V407 Cyg was discovered in outburst at 7th magnitude by Nishiyama et al. (2010) on 2010 March 10, in stark contrast to occasional brightenings observed over the years by a few magnitudes compared to historical low states in the range 13–17 m_{pg} . The binary comprises a white dwarf (WD) and Mira-type M6–7 red gi-

ant pulsating with a period of 763d, with an orbital period of 43 yr (Munari et al. 1990; Kolotilov et al. 2003). Spectroscopy obtained by Munari et al. (2011) and C. Buil¹ two days after outburst showed very broad Balmer lines; Munari et al. (2011) reported a full-width at half-maximum (FWHM) of 2760 km s⁻¹ on day 2.3, and described the outburst as a He/N nova expanding within the wind of the

* E-mail: orlando@astropa.inaf.it

¹ <http://www.astrosurf.com/buil/v407cyg/obs.htm>

Mira companion, similar to the 2006 explosion of RS Oph (see A. Evans, M. F. Bode, T. J. O'Brien, & M. J. Darnley 2008, and references therein). SiO maser emission was found to decline dramatically after the burst, leading Deguchi et al. (2011) to conclude that the maser emitting regions were essentially wiped out in a time scale of two weeks by the propagation of the nova shock into the Mira envelope.

The RS Oph blast wave produced copious X-rays from at most 3 days after optical discovery, when it was first observed by *Swift* and *RXTE*, characterized by a steady decline thereafter (Sokoloski et al. 2006; Bode et al. 2006; Nelson et al. 2008; Drake et al. 2009). V407 Cyg also developed into an X-ray source, though somewhat more slowly, exhibiting a strong brightening at 20 days or so, a peak near 30 days and a steady decline. Shore et al. (2011) analyzed the *Swift* UV and X-ray lightcurves together with optical spectra obtained during the first three months of the eruption. Balmer lines showed steady secular narrowing (see also Munari et al. 2011), and lines of [Ca V], [Fe VII], [Fe X], and He II exhibited asymmetric profiles attributed to an aspherical expansion reminiscent of that diagnosed for RS Oph from X-ray lines by Drake et al. (2009).

While not nearly as bright as RS Oph in X-rays, V407 Cyg was in some ways even more remarkable, with a firm detection by the *Fermi* Large Area Telescope of variable γ -ray emission in the 0.1–10 GeV range on 2010 March 10—the same day as optical discovery—that persisted for two weeks (Abdo et al. 2010). This was the first ever γ -ray detection of a nova explosion and was attributed by Abdo et al. (2010) to π^0 production and subsequent decay resulting from collisions of protons accelerated in the shock. Lü et al. (2011) pointed out that short period symbiotic novae such as RS Oph are unlikely to produce γ -rays because of the fast evolution of the blast wave in the higher density environment closer in to the red giant, whereas long period systems such as V407 Cyg provide a much longer-lived accelerator. Razzaque et al. (2010) further noted that V407 Cyg could have been a detectable source of high energy neutrinos.

The outburst mechanism for novae is thermonuclear runaway on the WD triggered by the mass of accreted material exceeding a critical limit (Starrfield et al. 1985, 1988). In two earlier papers we have applied sophisticated hydrodynamic models to the nova explosions on RS Oph (Orlando et al. 2009) and U Sco (Drake & Orlando 2010) to provide key insights into the nature of the explosion and its environment. In both sets of models, circumbinary material proved crucial in explaining the observed X-ray emission while providing a degree of collimation to the explosions. Here we describe similar detailed hydrodynamic simulations of the V407 Cyg explosion, and pay particular attention to the effects of circumbinary gas density enhancement and the secondary Mira companion on the explosion. In Sect. 2 we describe the hydrodynamic model, the numerical setup, and the synthesis of X-ray emission; in Sect. 3 we discuss the results; and finally in Sect. 4 we draw our conclusions.

2 HYDRODYNAMIC MODELING

The blast wave was modeled by numerically solving the time-dependent fluid equations of mass, momentum, and en-

ergy conservation, including radiative losses described by an optically-thin plasma and thermal conduction; the latter incorporated the effects of heat flux saturation. Owing to the long timescale of the blast evolution, radiative losses and thermal conduction were found to be more important than in the cases of RS Oph (Orlando et al. 2009) and U Sco (Drake & Orlando 2010). The long evolution timescale of the blast coupled with large expansion velocities of a few thousand km s^{-1} rendered the spatial extent too large and computationally demanding to perform an extensive set of fully 3-dimensional (3D) hydrodynamic simulations while still resolving the structure of the immediate binary environment, even with many levels of adaptive mesh refinement. The computational cost is raised by the inclusion of thermal conduction that is solved explicitly, such a scheme being subject to a rather restrictive stability condition as the thermal conduction timescale is generally shorter than the dynamical one (e.g. Hujeirat & Camenzind 2000; Hujeirat 2005; Orlando et al. 2008, 2010).

Given the large computational cost required by 3D simulations, we adopted the following strategy: we first explored the wide parameter space of the model by adopting a 2-dimensional (2D) cylindrical coordinate system (r, z) and, therefore, assuming the system to be symmetrical with respect to the axis passing through the WD and the companion star; then, for the set of parameters found to best reproduce the observations, we relaxed the hypothesis of axisymmetry and performed a fully 3D simulation in cartesian geometry. The 2D and 3D models developed here are otherwise similar to the 3D models of Orlando et al. (2009) and Drake & Orlando (2010) and we refer to those works for further details. The calculations were performed using FLASH, an adaptive mesh refinement multiphysics code for astrophysical plasmas (Fryxell et al. 2000) extended with additional computational modules to handle radiative losses and thermal conduction (see Orlando et al. 2005 for the details of the implementation). The hydrodynamic equations for compressible gas dynamics are solved using the FLASH implementation of the piecewise-parabolic method (PPM; Colella & Woodward 1984).

We adopted the system parameters of Munari et al. (1990); these are listed in Table 1. For the hydrodynamic models, the most important system parameters are the orbit semi-major axis, the wind mass loss rate and wind terminal velocity. These determine the gas density into which the blast occurs, and for a given explosion energy largely control the subsequent evolution timescale of the resulting shock wave system. The mass loss rate and terminal velocity are based on the data of Knapp & Morris (1985), while the orbital separation was estimated based on dust extinction changes assumed connected with orbital modulation. Munari et al. (1990) estimated orbital separations of 14.0, 15.5 and 16.4 AU for WD masses $M_{\text{WD}} = 0.5, 1.0$ and $1.4 M_{\odot}$, respectively; we adopt 15.5 AU and $M_{\text{WD}} = 1.0 M_{\odot}$. We also adopted the Munari et al. (1990) distance of 2.7 kpc, derived from the Glass & Feast (1982) luminosity vs. pulsation period relation extrapolated to the V407 Cyg period of 745 days.

Figure 1 shows an example of the initial conditions adopted in our simulations. The thermonuclear explosion is initiated by a spherical Sedov-type blast wave (Sedov 1959) centered on the WD, with radius $r_0 = 10^8$ km (red circle

Table 1. Adopted parameters and initial conditions for the hydrodynamic models of the 2010 V407 Cyg explosion

Parameter	Value							
Secondary star radius	$R_{\text{cs}} = 2.2 \text{ AU}$							
Binary separation	$a = 15.5 \text{ AU}$							
Orbital period	$P = 43 \text{ yr}$							
Spatial domain	(2D cylindrical)		(3D cartesian)					
	$0 \leq r \leq 530 \text{ AU}$		$-530 \leq x \leq 530 \text{ AU}$					
	$-530 \leq z \leq 530 \text{ AU}$		$0 \leq y \leq 530 \text{ AU}$					
			$0 \leq z \leq 530 \text{ AU}$					
AMR max. resolution	$5 \times 10^{11} \text{ cm}$ ($3.33 \times 10^{-2} \text{ AU}$)							
Time covered	0–60 days							
Model abbreviation	geometry	E_0 [erg]	M_{ej} [M_{\odot}]	n_{w} [cm^{-3}]	n_{cde} [cm^{-3}]	l_1 [AU]	l_2 [AU]	l_3 [AU]
E44.3-NW7	2D cylindrical	2×10^{44}	2×10^{-7}	10^7	—	—	—	—
E44.3-NW8	2D cylindrical	2×10^{44}	2×10^{-7}	10^8	—	—	—	—
E44.3-NW9	2D cylindrical	2×10^{44}	2×10^{-7}	10^9	—	—	—	—
E45-NW8	2D cylindrical	10^{45}	10^{-6}	10^8	—	—	—	—
E45-NW9	2D cylindrical	10^{45}	10^{-6}	10^9	—	—	—	—
E46-NW9	2D cylindrical	10^{46}	10^{-5}	10^9	—	—	—	—
E46.6-NW9	2D cylindrical	5×10^{46}	5×10^{-5}	10^9	—	—	—	—
E47-NW10	2D cylindrical	10^{47}	10^{-4}	10^{10}	—	—	—	—
E44-NW7-CDE6-L40	2D cylindrical	10^{44}	10^{-7}	10^7	10^6	40	40	—
E44-NW7-CDE6.7-L40	2D cylindrical	10^{44}	10^{-7}	10^7	5×10^6	40	40	—
E44-NW7-CDE7-L40	2D cylindrical	10^{44}	10^{-7}	10^7	10^7	40	40	—
E44.3-NW7-CDE6.3-L20	2D cylindrical	2×10^{44}	2×10^{-7}	10^7	2×10^6	20	20	—
E44.3-NW7-CDE6.3-L40	2D cylindrical	2×10^{44}	2×10^{-7}	10^7	2×10^6	40	40	—
E44.3-NW7-CDE6.3-L80	2D cylindrical	2×10^{44}	2×10^{-7}	10^7	2×10^6	80	80	—
E44.7-NW7-CDE6.7-L40	2D cylindrical	5×10^{44}	5×10^{-7}	10^7	5×10^6	40	40	—
E45-NW7-CDE6-L40	2D cylindrical	10^{45}	10^{-6}	10^7	10^6	40	40	—
E45-NW7-CDE6.7-L40	2D cylindrical	10^{45}	10^{-6}	10^7	5×10^6	40	40	—
E45-NW7-CDE7-L40	2D cylindrical	10^{45}	10^{-6}	10^7	10^7	40	40	—
3D-E44.3-NW7-CDE6.3	3D cartesian	2×10^{44}	2×10^{-7}	10^7	2×10^6	53	53	27

on the right in the inset panel of Fig. 1). In analogy with supernova explosions, the total energy of the blast, E_0 , is partitioned so that most of the explosion energy is kinetic (in particular we assumed 1/4 of the energy contained in thermal energy and the other 3/4 in kinetic energy as representative; e.g. Dohm-Palmer & Jones 1996). The total mass of the ejecta is M_{ej} . The blast propagates through the extended outer atmosphere (the wind) of the Mira companion and is off-set from the origin of the wind density distribution by 15.5 AU (i.e. the system orbital separation; see inset panel of Fig. 1). We assumed the gas density in the wind is proportional to R^{-2} (where R is the radial distance from the Mira). In addition to the R^{-2} density distribution, we also included a circumstellar envelope (or a circumbinary density enhancement in the wind, hereafter CDE), as predicted by detailed hydrodynamic modeling (e.g. Mastrodemos & Morris 1999; Walder et al. 2008). In particular, in systems comprising a red giant star, these models predict a CDE created by gravitational accumulation of the cool red giant wind toward the WD and a spiral shock wave caused by the motion of the stars through this gas. This scenario is also supported by observations in different wavelength bands of similar nova outbursts as, for instance, RS Oph (e.g. O’Brien et al. 2006; Bode et al. 2007; Rupen et al. 2008; Drake et al. 2009). In cartesian geometry, the mass density distribution of the unperturbed circumstellar medium (CSM) is given by:

$$\rho = \rho_w \left(\frac{R_{\text{cs}}}{R} \right)^2 + \rho_{\text{cde}} e^{[-(x/l_1)^2 - (y/l_2)^2 - (z/l_3)^2]} \quad (1)$$

where $\rho_w = \mu m_{\text{H}} n_w$ is the wind mass density close to the surface of the Mira companion, $\mu = 1.3$ is the mean atomic mass (assuming cosmic abundances), m_{H} is the mass of the hydrogen atom, R_{cs} is the radius of the Mira, R is the radial distance from the Mira, $\rho_{\text{cde}} = \mu m_{\text{H}} n_{\text{cde}}$ is the density enhancement close to the Mira, and l_1 , l_2 and l_3 are characteristic length scales determining the size and shape of the CDE. As examples, Fig. 2 shows the density profiles along the x axis for a model including the CDE (run 3D-E44.3-NW7-CDE6.3) and for a model without a CDE (run E44.3-NW7). The Mira companion is included in the calculation as an impenetrable body with radius $R_{\text{cs}} = 2.2 \text{ AU}$ (i.e. $\approx 500 R_{\odot}$; white circle on the left in the inset panel of Fig. 1).

In the 3D simulation, the hydrodynamic equations were solved in one quadrant of the whole spatial domain with the coordinate system oriented in such a way that both the WD and the companion star lie on the x axis (see Fig. 1; see also Drake & Orlando 2010 for more details). The companion is at the origin of the coordinate system, $(x, y, z) = (0, 0, 0)$, and the computational domain extends 1060 AU in the x direction and 530 AU in both the y and z directions; the WD is located to the right on the x axis ($y = z = 0$) at $x = 15.5 \text{ AU}$. We imposed reflecting boundary conditions at $y_{\text{min}} = 0$ and $z_{\text{min}} = 0$ (consistent with the adopted sym-

metry) and outflow (zero-gradient) conditions at the other boundaries.

Our 2D simulations considered a slab corresponding to the (x, z) plane of the 3D simulation, and the hydrodynamic equations were solved in one half of the 2D spatial domain, taking advantage of the symmetry of the configuration. In particular, assuming axisymmetry about the axis passing through the companion star and the WD, the cylindrical coordinate system was oriented in such a way that both the donor star and the WD lie on the z axis, with the former at the origin of the coordinate system, $(r, z) = (0, 0)$, and the latter at $z = 15.5$ AU. Since both the donor star and the initial nova remnant lie on the symmetry axis they are modelled as spheres in the cylindrical coordinate system. The computational domain extended 530 AU in the r direction, and 1060 AU in the z direction. The adopted geometrical system configuration implied imposition of an axisymmetric (reflecting) boundary condition at $r_{\min} = 0$ and outflow conditions at the remaining boundaries.

In order to compare the results of the 2D simulations with those derived from the 3D simulation, we reconstructed the 3D spatial distributions of all the physical variables (e.g. mass density and temperature) derived with the 2D simulations, by rotating the 2D slab about the z axis, according to the symmetry of the problem. Thus we passed from the cylindrical coordinate system to the cartesian one, orienting the cartesian coordinate system in such a way that both the WD and the companion star lie on the x axis, as in the 3D simulation.

The explosion and subsequent blast wave was followed for a total of 60 days in order to explore the evolution of the X-ray emission and study the effects of the circumstellar environment on the evolution of the blast during the evolutionary phase that was characterized by a pronounced peak of X-ray emission in the 2010 outburst (Shore et al. 2011). As with the modeling of the U Sco blast, the small scale of the stellar system compared with the size of the rapidly expanding blast wave over the 60 day period of interest presents a major computational challenge. To this end, we exploited the adaptive mesh capabilities of the FLASH code by using 12 nested levels of adaptive mesh refinement, with resolution increasing twice at each refinement level. This grid configuration yielded an effective maximum resolution of $\approx 5 \times 10^6$ km at the finest level, corresponding to ≈ 20 grid points per initial radius of the blast and ≈ 66 grid points per radius of the Mira companion. The calculations were performed using an automatic mesh derefinement scheme in the whole spatial domain except in the Mira (where the resolution does not vary during the blast evolution) that kept the computational cost approximately constant as the blast expanded. The effective mesh size was 16384×32768 for the 2D simulations, and $32768 \times 16384 \times 16384$ for the 3D simulation.

Solar abundances of Grevesse & Sauval (1998) (GS) were assumed for the wind and circumstellar density enhancement, while ejecta metal abundances were assumed to be enhanced by a factor of ten. This latter choice was guided by the *Swift* spectra that Shore et al. (2011) found to be rich in both N and O—by possibly more than a factor of ten—and by observations of He-rich ejecta in the outburst of U Sco (see Drake & Orlando 2010), as well as the Drake et al. (2009) high-resolution X-ray spectroscopic study of the 2006 RS Oph blast that found evidence for

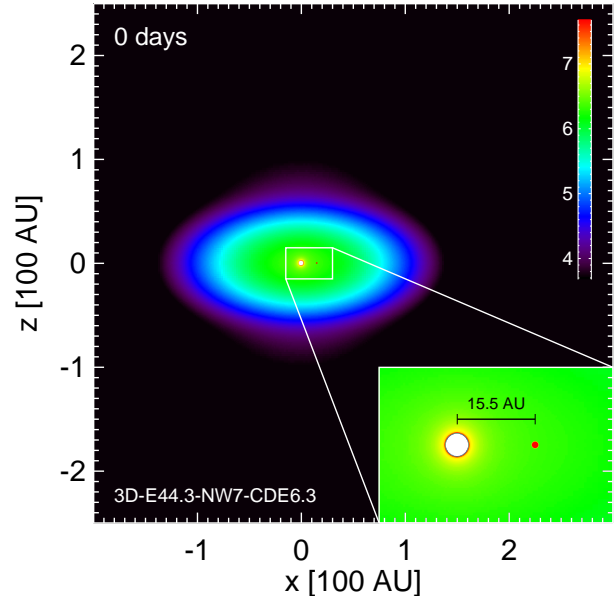


Figure 1. Colour-coded cross-section image of the gas density distribution, on a logarithmic scale, in units of cm^{-3} , showing the initial conditions of run 3D-E44.3-NW7-CDE6.3. The inset panel shows a close-up view of the initial geometry of the V407 Cyg system. The companion star is at the origin (white circle on the left of the inset), and the white dwarf lies on the x axis at $x = 15.5$ AU (red circle on the right).

metal-rich ejecta. The adopted abundances are relevant for the radiative losses from shocked ejecta, and for the local absorption by the shocked CSM (with GS abundances) and by the ejecta (with GS abundances $\times 10$) encountered within the blast wave. The choice of abundances is also relevant for computation of the emitted X-ray intensity of the blast. Such emission was synthesized from the model results using the methodology described by Orlando et al. (2009). The synthesis includes: thermal broadening of emission lines, Doppler shift of lines due to the component of plasma velocity along the line-of-sight, photoelectric absorption by the interstellar medium (ISM), CSM, and ejecta. The absorption by the ISM was calculated assuming a column density $N_{\text{H}} = 2 \times 10^{21} \text{ cm}^{-2}$; the local absorption was calculated self-consistently from the distributions of shocked CSM and shocked ejecta.

The influence of the different system parameters was investigated through the 2D simulations, by exploring models with an initial energy of explosion, E_0 , in the range $10^{44} - 10^{47}$ erg, ejecta mass, M_{ej} , in the range $10^{-7} - 10^{-4} M_{\odot}$, wind density in the range $10^7 - 10^{10} \text{ cm}^{-3}$, CDE density in the range $10^6 - 10^7 \text{ cm}^{-3}$ (see Table 1). The ranges of ejected mass and outburst energy include those typical of recurrent novae ($10^{-7} < M_{\text{ej}} < 10^{-6} M_{\odot}$, $10^{44} < E_0 < 10^{45}$ erg), given the close similarities between the 2010 outburst of V407 Cyg and those of RS Oph and U Sco, and the ranges typical of classical novae ($10^{-5} < M_{\text{ej}} < 10^{-4} M_{\odot}$, $10^{46} < E_0 < 10^{47}$ erg; e.g. Bode 2010). In the 2D simulations, the CDE has a spherical shape (according to the symmetry of the system) and Eq. 1 reduces to

$$\rho = \rho_w \left(\frac{R_{\text{cs}}}{R} \right)^2 + \rho_{\text{cde}} e^{[-(r/l_1)^2 - (z/l_2)^2]} \quad (2)$$

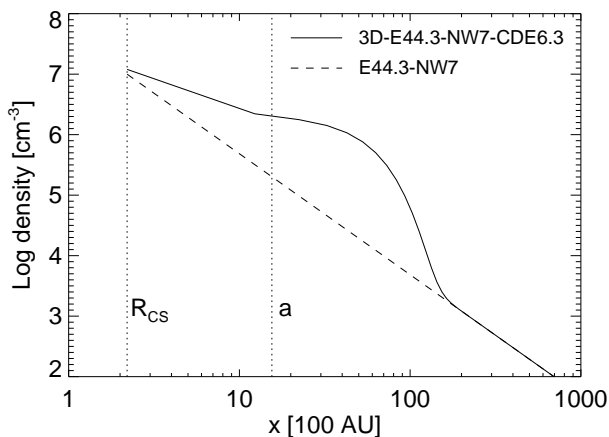


Figure 2. Initial density profiles along the x axis for a model including the CDE (run 3D-E44.3-NW7-CDE6.3; solid line) and for a model without CDE (run E44.3-NW7; dashed line). The dotted lines mark the radius of the Mira companion, R_{cs} , and the binary separation, a .

with $l_1 = l_2$. The CDE thickness was explored in the range 20–80 AU. The additional 3D simulation allowed us to study the collimation of the ejecta due to an equatorial density enhancement: in this case we adopted the parameters of the 2D simulation that best fit the observations and explored the effects of a disk-like CDE (according to Walder et al. 2008) on the blast evolution, by assuming $l_1 = l_2$ and $l_3 < l_1$ in Eq. 1.

3 RESULTS AND DISCUSSION

3.1 Hydrodynamic evolution

The V407 Cyg models show a blast wave evolution that is in some ways intermediate between those presented for RS Oph by Orlando et al. (2009) and for U Sco by Drake & Orlando (2010). The WD of V407 Cyg is characterized by the massive circumstellar gas envelope of its Mira companion in which it sits, similar to the WD of RS Oph located within the dense wind of its red giant secondary, with no evident well-defined accretion disk (unlike U Sco). V407 Cyg has a much wider orbital separation than RS Oph and U Sco, implying that the nova explodes initially into a relatively low density environment, as in the case of U Sco, despite the presence of the CDE. The size of the Mira companion ($R_{cs} = 2.2$ AU) is significant compared to the size of the system, so that the Mira partially shields the blast, as found in U Sco.

The evolution of the blast for three representative V407 Cyg models is illustrated in Fig. 3. Post-blast gas density distributions in the (x, z) plane bisecting the system (the plane of the orbital axis; the equatorial plane is edge on) are shown, sampled at the labeled times. The figure also shows the distribution of ejecta within the blast wave by highlighting regions where more than 90% of the mass is material ejected in the explosion (dashed contours). The hot post-shock plasma is dominated by thermal conduction rather than radiative cooling, and this partially suppresses the hydrodynamic instability that would otherwise develop during the evolution of the blast wave (see Orlando et al.

2005, 2008). Owing to the low density environment in which the blast propagates, and to the high post-shock temperature, there are in fact no regions within the blast that appear dominated by radiative losses. Thermal conduction is expected to dominate over radiative cooling when the conduction time-scale is shorter than the cooling time-scale or, in other words, in plasma structures with a length-scale smaller than the Field length, $L_F \approx 10^6 T^2 / n_H$ (Begelman & McKee 1990; Orlando et al. 2005), where T and n_H are the plasma temperature and particle number density, respectively. For our models, $L_F \approx 240$ AU, such that this length-scale is larger than the size of the plasma structures produced in the blast.

The models all show aspherical shock morphologies, rendered by the blast wave propagating through the inhomogeneous circumstellar gas distribution. In models without a CDE (hereafter NOCDE models; e.g. run E44.3-NW8 in Fig. 3), the aspherical morphology is mainly due to the offset of the blast wave with respect to the origin of the wind density distribution. A similar morphology is found in models including a spherical CDE (hereafter SPHCDE models) with an origin coincident with that of the wind density distribution (e.g. run E44.3-NW7-CDE6.3-L40 in Fig. 3). Here again the morphology is determined by the off-set of the blast wave with respect to the origin of the CDE. At variance with NOCDE models, however, the blast initially propagates in a medium with a density distribution decreasing away from the companion star more slowly than the R^{-2} wind density distribution (see Fig. 2).

The CDE has quite an important effect on the blast evolution if its shape is disk-like, as in run 3D-E44.3-NW7-CDE6.3 (see right panels in Fig. 3). In this case, the blast morphology is similar to that found from the modeling of the RS Oph outburst (Walder et al. 2008; Orlando et al. 2009): both the blast and ejecta are strongly collimated in polar directions, leading to a bipolar shock morphology. It is remarkable that the shock expansion at day 30 is almost parallel to the z -axis. Figure 4 shows, as an example, the collimation of blast and ejecta 60 days after the outburst for the model 3D-E44.3-NW7-CDE6.3. A similar poleward blast collimation was a feature of hydrodynamic simulations of the early U Sco blast (Drake & Orlando 2010); there, the collimation was caused by a dense accretion disk surrounding the WD. Such a blast collimation is also suggested by observations. Indeed, collimation signatures found during the 2006 RS Oph outburst at radio, infrared, optical, and X-ray wavelengths (O’Brien et al. 2006; Bode et al. 2006; Chesneau et al. 2007; Luna et al. 2009; Drake et al. 2009) represent a growing consensus in the literature that blast collimation is a common feature of nova outbursts.

In all the models, the shock front propagating toward the Mira companion is partially shielded by it and refracted around it. As a result, the shock converges on the rear side of the companion star, undergoing a conical self-reflection there, and producing a wake with relatively dense ($n_H \approx 10^6$ cm $^{-3}$) and hot ($T \approx 5 \times 10^7$ K) post-shock plasma. We expect, therefore, that this structure may lead to conspicuous observable X-ray emission. The potential for such a structure to explain persistent blue-ward extension of optical emission lines was also suggested by Shore et al. (2011). At early stages, the secondary star also gives rise to a bow shock with a temperature $T \approx 10^7$ K. However, this feature

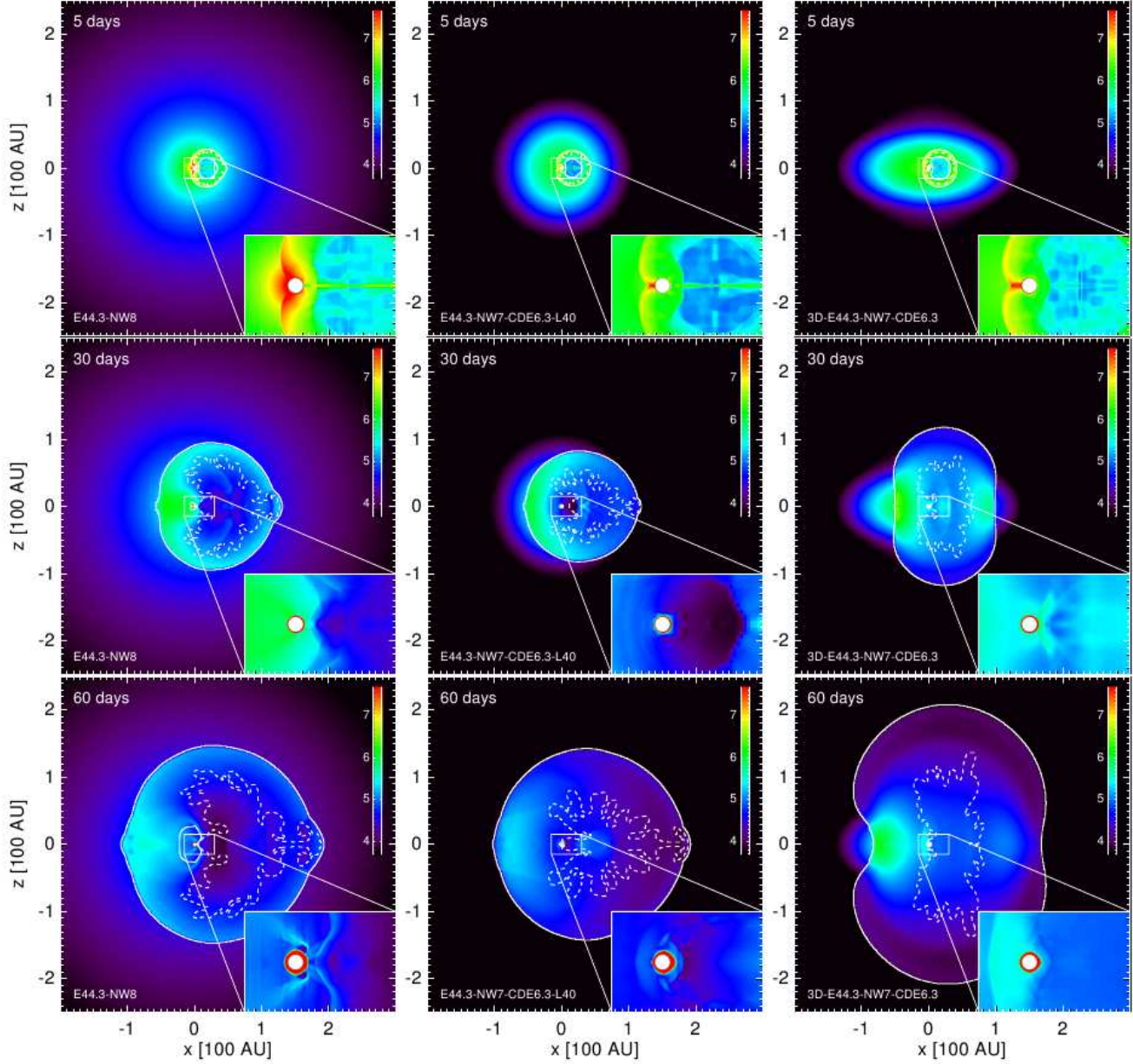


Figure 3. Cross-section images of the gas density distribution, on a logarithmic scale in units of cm^{-3} (see the color table in the upper right corner of each panel), sampled at the labeled times for three representative V407 Cyg models. The Mira companion is at the origin and the WD is off-set from the origin to the right by 15.5 AU. The different panels illustrate the evolution of the blast for a model without CDE (run E44.3-NW8; left panels), for a model with a spherical CDE (run E44.3-NW7-CDE6.3-L40; center panels), and for a model with a disk-like CDE (run 3D-E44.3-NW7-CDE6.3; right panels). Inset panels show the blast structure closer to the system origin. The white circle in the inset represents the Mira companion. The white dashed contour encloses the ejecta. The white solid contour denotes the regions with plasma temperature $T > 10^6$ K.

is characterized by relatively low densities ($n_{\text{H}} \approx 10^5 \text{ cm}^{-3}$; one order of magnitude lower than the density in the wake) and we expect only a modest contribution to X-ray emission.

3.2 X-ray emission

From the simulations, we synthesized the X-ray emission in the $[0.6 - 12.4]$ keV band, using the method described by Orlando et al. (2009) and outlined in Sect. 2. Fig. 5 shows the maps of X-ray emission projected along the line of sight

at day 30 (namely when a pronounced peak of X-ray emission was observed in the 2010 outburst) for the models shown in Fig. 3. The maps are shown on linear (upper panels) and logarithmic (lower panels) scales to highlight structures with very different emission levels. The plane of the orbit of the central binary system lies on the (x, y) plane and is assumed to be edge on. In all cases, most of the X-ray emission arises from the high-temperature shocked CSM in the wake produced by the convergent shock on the rear side of the companion star. Similar plasma structures have been

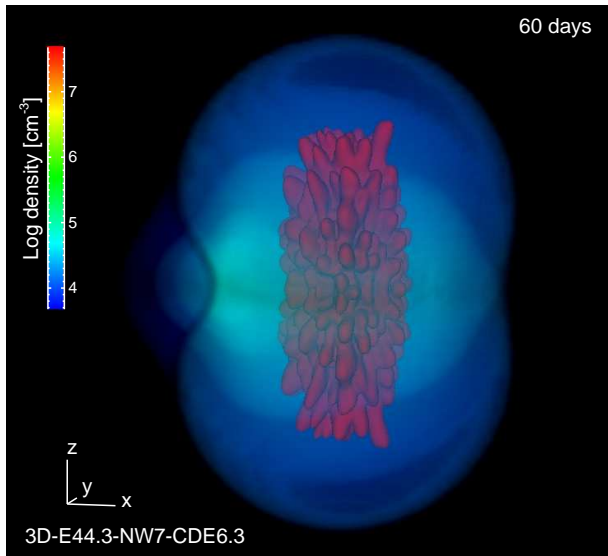


Figure 4. Three-dimensional rendering of particle number density, on a logarithmic scale, in units of cm^{-3} (see color table in the upper left corner of the panel), at day 60 for the model 3D-E44.3-NW7-CDE6.3. The ejecta are highlighted in red. The plane of the orbit of the central binary system lies on the (x, y) plane.

found in numerical simulations describing the outburst of RS Oph (e.g. Walder et al. 2008) and are generally expected as a result of the shielding of the blast by the companion star.

The X-ray lightcurves of the simulations in the $[0.6 - 12.4]$ keV band are shown in Fig. 6, together with the observed lightcurve. The latter was based on the *Swift*/XRT count rates reported by Shore et al. (2011), considering a maximum X-ray luminosity of $L_X = 1.2 \times 10^{34} \text{ erg s}^{-1}$ at a distance of 2.7 kpc (Shore et al. 2011). As found for U Sco by Drake & Orlando (2010), in NOCDE models (left panel in Fig. 6) in general the X-ray luminosity, L_X , is larger for higher explosion energy (and ejecta mass), and wind gas density. For outburst energies and ejecta masses in the range of values typically observed for recurrent novae (i.e. $10^{-7} < M_{\text{ej}} < 10^{-6} M_{\odot}$, $10^{44} < E_0 < 10^{45} \text{ erg}$; e.g. Bode 2010), the synthetic L_X reaches its maximum very quickly, within few days after the explosion, so that none of these lightcurves fit the observed one which is characterized by a maximum around day 30. On the other hand, assuming outburst energies and ejecta masses typical of classical novae (i.e. in the ranges $10^{-5} < M_{\text{ej}} < 10^{-4} M_{\odot}$, $10^{46} < E_0 < 10^{47} \text{ erg}$; e.g. Bode 2010), the peak of X-ray emission can be reached at later times. Among these models, that which best reproduces the X-ray peak at day 30 is E46.6-NW9 (orange line in the left panel in Fig. 6), although it fails in reproducing the descending slope of the observed lightcurve. This model predicts outburst energy of the order of $\approx 5 \times 10^{46} \text{ erg}$ and mass of ejecta $\approx 5 \times 10^{-5} M_{\odot}$ that seem to be too high in the case of V407 Cyg that shows many similarities with the novae RS Oph and U Sco.

In the presence of a CDE, the X-ray luminosity mainly depends on the physical characteristics of the density enhancement: the greater the size and gas density of the CDE, the larger L_X (central and right panels in Fig. 5). In these models, the blast reaches its maximum X-ray luminosity

later than in NOCDE models, and the time of maximum depends on the size and gas density of the CDE and on the explosion energy (and ejecta mass). In particular, the time delay of maximum X-ray luminosity is longer for lower gas density and greater size of the CDE, and for higher explosion energy. Among the SPHCDE models, that which best reproduces the observations is E44.3-NW7-CDE6.3-L40 (blue line in the right panel of Fig. 6): it describes a continuous rise of X-ray luminosity up to a maximum of $L_X \approx 2 \times 10^{34} \text{ erg s}^{-1}$ at day 30 and then a subsequent decay phase until day 60, with the same slope as the observed lightcurve. It is worth noting that this model assumes outburst energies and ejecta masses in the range of values typically observed for recurrent novae, while the “best-fit” NOCDE model assumes values typical of classical novae. For E44.3-NW7-CDE6.3-L40, we extended the simulation in order to cover the whole period in which the observed lightcurve is defined. We found that, after day 60, the synthetic lightcurve fades faster than the observations which seem to be characterized by a plateau between days 60 and 90. This discrepancy could be explained as being due to the details of the density structure of the CDE; for instance, a radial density profile of the CDE decreasing away from the companion star slower than that modelled here may change the descending slope of the lightcurve. Another possible cause of the discrepancy may be some departures from the simple wind density profile adopted here.

The effect of the shape of the CDE on the synthetic X-ray image and lightcurve was explored by performing a 3D simulation describing a disk-like CDE (run 3D-E44.3-NW7-CDE6.3; see right panels in Fig. 3) with the same parameters of run E44.3-NW7-CDE6.3-L40 but with $l_1 = l_2 = 53$ and $l_3 = 27$ in Eq. 1 (see Table 1). In this case, again most of the X-ray emission originates in the high-temperature shocked plasma in the wake of the companion star (see right panels in Fig. 5), although the X-ray source here is more compact than in run E44.3-NW7-CDE6.3-L40. The X-ray lightcurve derived from run 3D-E44.3-NW7-CDE6.3 is illustrated in the right panel of Fig. 6 (magenta line): the curve is similar to that derived from run E44.3-NW7-CDE6.3-L40 and is in good agreement with the observed lightcurve.

4 SUMMARY AND CONCLUSIONS

We have modeled the first 60 days of evolution of the 2010 blast wave of the nova V407 Cyg. The models explore the 3D structure of the blast wave originating from the nova outburst, taking into account simultaneously the radiative cooling and thermal conduction (including heat flux saturation). Our analysis indicates the following:

- (i) the blast wave and the ejecta distribution are both aspherical due to the inhomogeneous CSM in which the blast expands;
- (ii) in case of a disk-like CDE, the blast and the ejecta are collimated in polar directions, leading to a bipolar shock morphology;
- (iii) the shock front propagating toward the Mira is partially shielded by it, producing a wake with dense and hot post-shock plasma on the rear side of the companion star;
- (iv) during the evolution of the blast, most of the X-ray

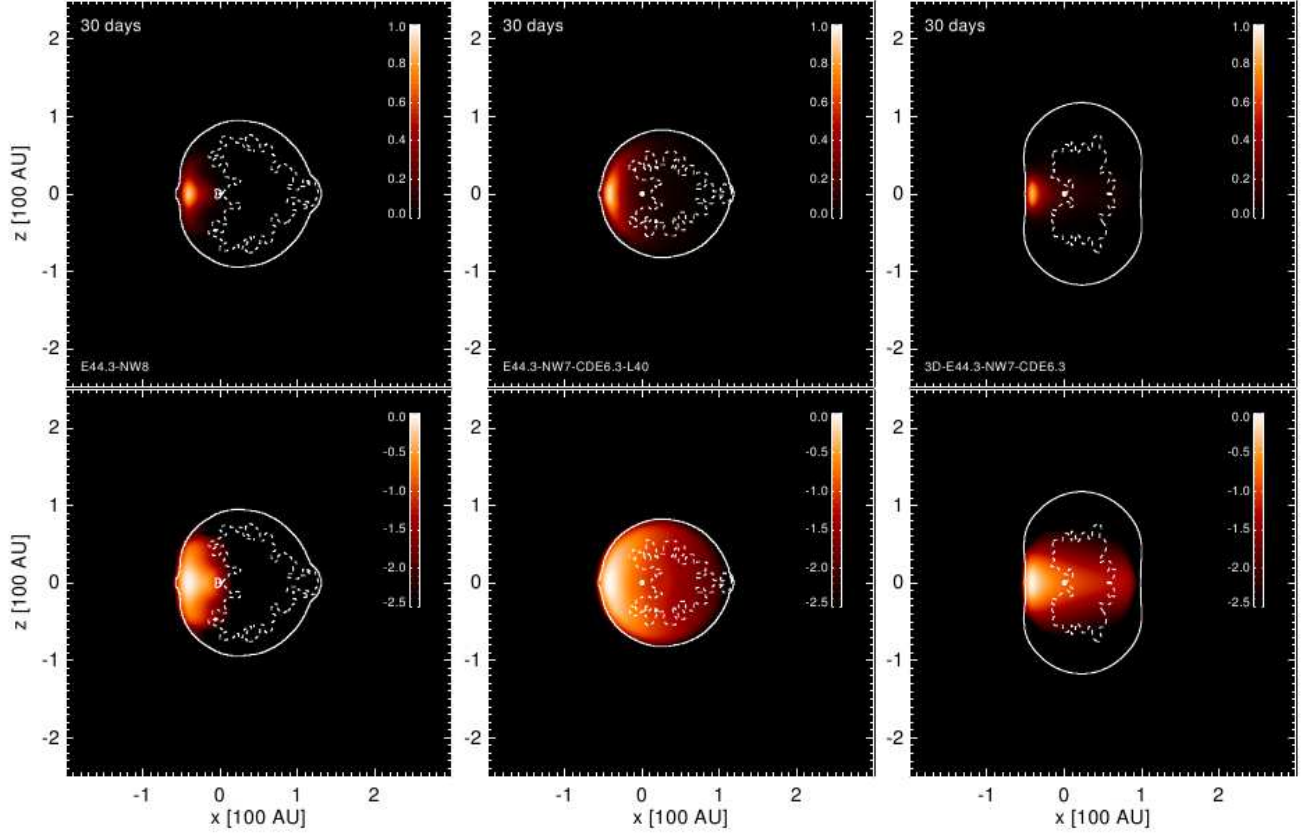


Figure 5. X-ray images (normalized to the maximum of each panel) in $[0.6 - 12.4]$ keV band projected along the line of sight of the blast after 30 days of evolution, corresponding to the density distributions in the middle panels in Fig. 3. Upper panels are rendered with a linear surface brightness scale and lower panels with a logarithmic scale. Both the Mira companion and the WD lie on the x -axis. The plane of the orbit is edge on. Most of the X-ray emission originates from the shocked CSM. The white dashed contour encloses the ejecta. The white solid contour denotes the forward shock.

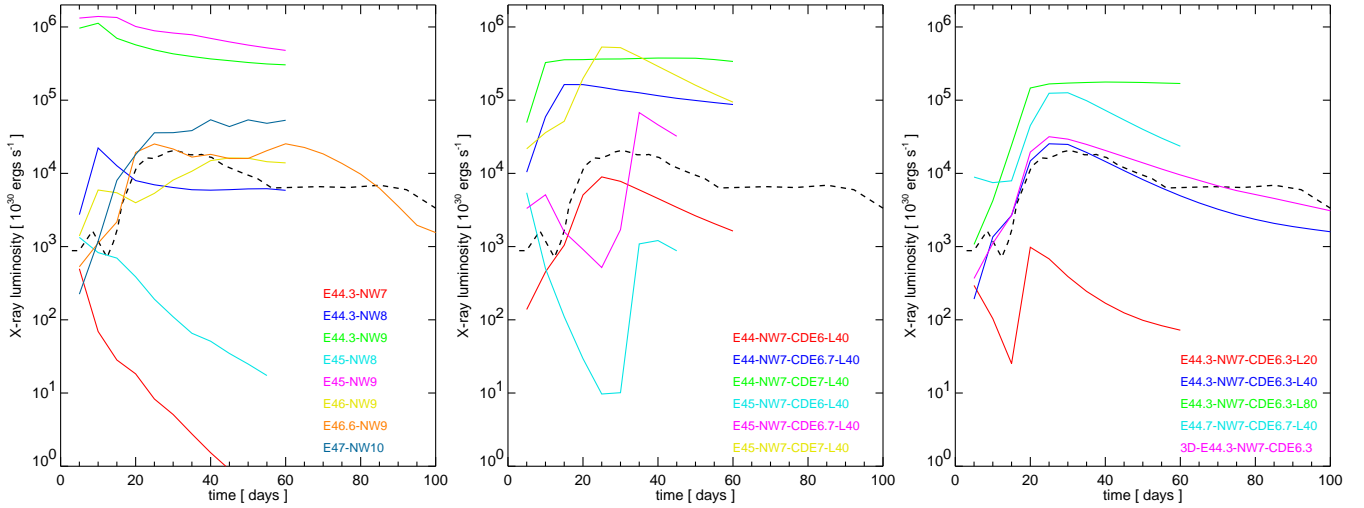


Figure 6. X-ray lightcurves in the $[0.6 - 12.4]$ keV band originating from the nova outburst (colour-coded solid lines) for the models reported in Table 1. The left panel shows the results for the NOCDE models. The X-ray flux is obtained by integrating the synthetic X-ray emission in the whole spatial domain and takes into account the effects of local absorption by shocked CSM and ejecta. The reference black dashed line is the observed lightcurve reported by Shore et al. (2011).

emission arises from the dense and hot post-shock plasma in the wake of the companion star;

(v) the observed X-ray lightcurve can be reproduced without including the CDE in the model only if the outburst energy and ejected mass were of the same order of magnitude as those at the upper end of ranges for classical novae, namely $M_{\text{ej}} \approx 5 \times 10^{-5} M_{\odot}$ and $E_0 \approx 5 \times 10^{46}$ erg, i.e. values much higher than those estimated in the case of RS Oph and U Sco;

(vi) the model best reproducing the observations assumes the presence of a CDE and suggests that the explosion energy in the 2010 outburst was $\approx 2 \times 10^{44}$ erg (and the mass of ejecta $\approx 2 \times 10^{-7} M_{\odot}$, i.e. values comparable to those estimated for RS Oph and U Sco) and that the blast propagated through a CDE with radius of the order of 40 AU and gas density $\approx 2 \times 10^6 \text{ cm}^{-3}$.

Shore et al. (2011) note that the 2010 outburst of V407 Cyg closely resembles the spectroscopic development of RS Oph which is considered the prototype of symbiotic-like recurrent novae. This fact has suggested that V407 Cyg could belong to the same class of recurrent novae, although its outburst was the first recorded nova event for this system. On the other hand, as discussed by Shore et al. (2011) the historical lightcurve of V407 Cyg is characterized by many gaps and it is possible that outbursts similar to that observed in 2010 were missed. Munari et al (1990) estimated an accretion rate of $\sim 10^{-8} M_{\odot} \text{ yr}^{-1}$ for a WD mass of $M_{\text{WD}} \sim 1 M_{\odot}$. If this accreted mass were ejected in the nova event, our estimate of the ejecta mass for the CDE case implies a recurrence time for nova events of 20 years or so. For this accretion rate, the recurrence timescale is consistent with higher mass white dwarfs (e.g. $M_{\text{WD}} \sim 1.25 M_{\odot}$; e.g. Prialnik & Kovetz 1995). Within the fairly large uncertainties of accretion rate and ejecta mass estimates, this is consistent with either a scenario in which one or more outbursts have been missed, or with a recurrence timescale of the order of 100 years. For a low mass WD the recurrence timescale is two orders of magnitude longer.

In the light of the above considerations, and the results of numerical models showing that gas does accumulate in the orbital plane of a symbiotic binary², we suggest that the model best describing the 2010 outburst of V407 Cyg is that assuming the presence of a CDE and predicting outburst energy and mass of ejecta similar to those estimated for RS Oph (run 3D-E44.3-NW7- CDE6.3).

Finally, the X-ray structure predicted by our model has interesting implications for the line profiles expected to be observed during the outburst. Simulations of the 2006 outburst of RS Oph, that occurred close to orbital quadrature, have shown that most of the X-ray emission arises from a compact source propagating perpendicular to the line of sight, which is similar to that found here. This source produced asymmetric and slightly blue-shifted line profiles due to substantial X-ray absorption of red-shifted

emission by shocked material (Orlando et al. 2009). These model predictions were in nice agreement with the findings of Drake et al. (2009) who reported similar asymmetric line profiles from the analysis of *Chandra*/HETG observations of RS Oph. In the light of the above results, we expect therefore that even in the case of V407 Cyg the line profiles should be asymmetric and blue-shifted due to X-ray absorption of red-shifted emission by shocked material. Interestingly, Shore et al. (2011) reported asymmetric line profiles with extended blue wings during the 2010 outburst of V407 Cyg. These authors suggested that the emission and the asymmetric line profiles could originate in the wake produced by the convergent shock on the rear side of the companion star. We note that the scenario proposed by Shore et al. (2011) is compatible with the findings of the present paper.

ACKNOWLEDGMENTS

We thank an anonymous referee for useful suggestions. SO acknowledges support from the Italian Ministero dell'Università e Ricerca (MIUR) and from the Istituto Nazionale di Astrofisica (INAF). JJD was funded by NASA contract NAS8-39073 to the *Chandra X-ray Center* (CXC) during the course of this research and thanks the CXC director, Harvey Tananbaum, and the CXC science team for advice and support. The software used in this work was in part developed by the DOE-supported ASC/Alliance Center for Astrophysical Thermonuclear Flashes at the University of Chicago. The simulations were executed at the SCAN (Sistema di Calcolo per l'Astrofisica Numerica) facility for high performance computing at INAF – Osservatorio Astronomico di Palermo.

REFERENCES

- A. Evans, M. F. Bode, T. J. O'Brien, & M. J. Darnley ed. 2008, RS Ophiuchi (2006) and the Recurrent Nova Phenomenon Vol. 401 of Astronomical Society of the Pacific Conference Series
- Abdo A. A., Ackermann M., Ajello M., Atwood W. B., Baldini L., Ballet J., Barbiellini G., Bastieri D., Bechtol K., Bellazzini R., et al. 2010, *Science*, 329, 817
- Begelman M. C., McKee C. F., 1990, *Astrophys. J.*, 358, 375
- Bode M. F., 2010, *Astronomische Nachrichten*, 331, 160
- Bode M. F., Harman D. J., O'Brien T. J., Bond H. E., Starrfield S., Darnley M. J., Evans A., Eyres S. P. S., 2007, *Astrophys. J.*, 665, L63
- Bode M. F., O'Brien T. J., Osborne J. P., Page K. L., Senziani F., Skinner G. K., Starrfield S., Ness J.-U., Drake J. J., Schwarz G., Beardmore A. P., Darnley M. J., Eyres S. P. S., Evans A., Gehrels N., Goad M. R., Jean P., Krautter J., Novara G., 2006, *Astrophys. J.*, 652, 629
- Chesneau O., Nardetto N., Millour F., Hummel C., Domicianno de Souza A., Bonneau D., Vannier M., Rantakyro F., Spang A., Malbet F., Mourard D., Bode M. F., O'Brien T. J., Skinner G., Petrov R. G., Stee P., Tatulli E., Vakili F., 2007, *Astron. & Astrophys.*, 464, 119
- Colella P., Woodward P. R., 1984, *Journal of Computational Physics*, 54, 174

² The gravitational accumulation of gas toward the WD is expected to have for V407 Cyg a form similar to that for RS Oph. In fact, Walder et al. (2008) have characterized the density enhancement by the ratio $R = V_{\text{RG}}/V_{\text{orb}}$ (where V_{RG} is the terminal wind velocity and $V_{\text{orb}} = 2\pi a/P$, with P the orbital period) which for both RS Oph and V407 Cyg is of order 1.

- Deguchi S., Koike K., Kuno N., Matsunaga N., Nakashima J.-I., Takahashi S., 2011, *Publ. Astron. Soc. Japan*, 63, 309
- Dohm-Palmer R. C., Jones T. W., 1996, *Astrophys. J.*, 471, 279
- Drake J. J., Laming J. M., Ness J.-U., Orlando S., Starrfield S., Beardmore A. P., Bode M. F., Evans A., Eyres S. P. S., Gehrz R. D., Goad M. R., Gonzalez-Riestra R., Krautter J., O'Brien T. J., Osborne J. P., Page K. L., Schwarz G., Woodward C. E., 2009, *Astrophys. J.*, 691, 418
- Drake J. J., Orlando S., 2010, *Astrophys. J.*, 720, L195
- Fryxell B., Olson K., Ricker P., Timmes F. X., Zingale M., Lamb D. Q., MacNeice P., Rosner R., Truran J. W., Tufo H., 2000, *Astrophys. J. Suppl.*, 131, 273
- Glass I. S., Feast M. W., 1982, *Mon. Not. R. Astron. Soc.*, 199, 245
- Grevesse N., Sauval A. J., 1998, *Space Science Reviews*, 85, 161
- Hujeirat A., 2005, *Computer Physics Communications*, 168, 1
- Hujeirat A., Camenzind M., 2000, *Astron. & Astrophys.*, 362, L41
- Knapp G. R., Morris M., 1985, *Astrophys. J.*, 292, 640
- Kolotilov E. A., Shenavrin V. I., Shugarov S. Y., Yudin B. F., 2003, *Astronomy Reports*, 47, 777
- Lü G., Zhu C., Wang Z., Huo W., Yang Y., 2011, *Mon. Not. R. Astron. Soc.*, 413, L11
- Luna G. J. M., Montez R., Sokoloski J. L., Mukai K., Kastner J. H., 2009, *Astrophys. J.*, 707, 1168
- Mastrodemos N., Morris M., 1999, *Astrophys. J.*, 523, 357
- Munari U., Joshi V. H., Ashok N. M., Banerjee D. P. K., Valisa P., Milani A., Siviero A., Dallaporta S., Castellani F., 2011, *Mon. Not. R. Astron. Soc.*, 410, L52
- Munari U., Margoni R., Stagni R., 1990, *Mon. Not. R. Astron. Soc.*, 242, 653
- Nelson T., Orio M., Cassinelli J. P., Still M., Leibowitz E., Mucciarelli P., 2008, *Astrophys. J.*, 673, 1067
- Nishiyama K., Kabashima F., Kojima T., Sakaniwa K., Tago A., Schmeer P., Munari U., 2010, *IAU Circ.*, 9130, 1
- O'Brien T. J., Bode M. F., Porcas R. W., Muxlow T. W. B., Eyres S. P. S., Beswick R. J., Garrington S. T., Davis R. J., Evans A., 2006, *Nature*, 442, 279
- Orlando S., Bocchino F., Reale F., Peres G., Pagano P., 2008, *Astrophys. J.*, 678, 274
- Orlando S., Drake J. J., Laming J. M., 2009, *Astron. & Astrophys.*, 493, 1049
- Orlando S., Peres G., Reale F., Bocchino F., Rosner R., Plewa T., Siegel A., 2005, *Astron. & Astrophys.*, 444, 505
- Orlando S., Sacco G. G., Argiroffi C., Reale F., Peres G., Maggio A., 2010, *Astron. & Astrophys.*, 510, A71+
- Prialnik D., Kovetz A., 1995, *Astrophys. J.*, 445, 789
- Razzaque S., Jean P., Mena O., 2010, *Phys. Rev. D*, 82, 123012
- Rupen M. P., Mioduszewski A. J., Sokoloski J. L., 2008, *Astrophys. J.*, 688, 559
- Sedov L. I., 1959, *Similarity and Dimensional Methods in Mechanics*. New York: Academic Press, 1959
- Shore S. N., Wahlgren G. M., Augusteijn T., Liimets T., Page K. L., Osborne J. P., Beardmore A. P., Koubsky P., Šlechta M., Votruba V., 2011, *Astron. & Astrophys.*, 527, A98+
- Sokoloski J. L., Luna G. J. M., Mukai K., Kenyon S. J., 2006, *Nature*, 442, 276
- Starrfield S., Cox A. N., Kidman R. B., Pensnell W. D., 1985, *Astrophys. J.*, 293, L23
- Starrfield S., Sparks W. M., Shaviv G., 1988, *Astrophys. J.*, 325, L35
- Walder R., Folini D., Shore S. N., 2008, *Astron. & Astrophys.*, 484, L9